Effect of Space Environment on Structural Diagnostics

FUNMILOLA NWOKOCHA, ANDREI ZAGRAI
and MARY ANDERSON

ABSTRACT

Space structures such as rockets, spaceships, and satellites are subject to environmental factors depending on their mission. As mankind becomes more dependent on various space assets, understanding the behavior of structural components in space grows in importance. For commercial space transportation, three environments are of the most interest: suborbital, orbital and interplanetary. Currently, commercialization priorities are focused on suborbital and orbital applications. This contribution explores potential effects of suborbital and orbital environments on structural diagnostics of spaceships. The primary concern for suborbital flight is survivability of structure during launch and re-entry. This is when most of the dynamic loads occur which may cause mechanical failure of the spacecraft. In addition, the suborbital flight is characterized by high thermal loads occurring during re-entry. Given that during suborbital flight, spaceship spends only minutes in space, the contribution of actual space environment to such flight is minor with rather low radiation doses and stable temperature range. The environmental contribution changes when a structure is placed on low earth orbit (LEO). The temperature could vary between -120 ºC to +120 ºC in this orbit and this thermal variation could cause thermal fatigue on structures leading to formation of cracks. Absence of atmosphere (pressure in the order of a few micropascals) affects a vibration environment. Atomic oxygen (AO) considerably affects non-metallic materials, causing their deterioration on LEO. Materials on LEO are subject to UV, particulate and ionizing radiation with each of them being responsible for different deterioration mechanisms. Micrometeorites with speeds exceeding several km/s could cause notable damage. In this contribution, we study effect of space environment on piezoelectric-based SHM. Thermal effects are considered first, which are followed by the radiation environment. Results of laboratory experiments are presented along with the theoretical developments. Recommendations are suggested for utilization of SHM on LEO.

Department of Mechanical Engineering, New Mexico Institute of Mining and Technology, Socorro, NM 87801, U.S.A.

INTRODUCTION

Spacecraft are adversely affected by space environment. Though space is generally considered to be a benign environment, it contains numerous constituents which can lead to reduction of performance and catastrophic failures of structures. The space environment can be categorized into the neutral atmosphere, thermal environment, plasma, meteoroids and orbital debris, solar environment, ionizing radiation and magnetic field [1]. The greatest impact of the space environment on the low earth orbit (LEO) is from the neutral atmosphere, debris, direct sunlight and trapped radiation. The interaction of spacecraft electronic and mechanical systems with space environment is the major cause of spacecraft failures [1]. Many spacecraft materials are susceptible to attacks by atomic oxygen which can be aggravated by their simultaneous exposure to other factors in space, leading to a serious deterioration of their mechanical, optical and thermal properties [1, 2].

In this contribution we explore the effect of space environment on structural diagnostics in suborbital flights and on LEO.

EFFECTS OF SUBORBITAL SPACE ENVIRONMENT ON STRUCTURAL COMPONENTS

A suborbital spacecraft flies at a speed below the orbital velocity and almost all external conditions changes during a typical suborbital flight [3, 4]. The environmental effects of the suborbital space on structures should be considered.

Rocket Spinning: Many rockets are designed to spin as soon as they are launched into the suborbital space so that the effect of weathercocking (wind, gravity) and its own thrust are mitigated. A spinning rocket is slow to react to disturbances and when it does react, it does not swing excessively. As a result, the rocket maintains its intended trajectory. The angular velocity of a typical model rocket at constant airspeed rises from 0 to approximately 150 rad/sec [5].

Acoustic Load: During launch, spacecraft encounter significant external excitation from acoustic and structural vibrations caused by engine exhaust gases. Acoustic pressure fluctuations on the spacecraft fairing lead to high noise levels and potential damage to the structure and payload. The highest acoustic loads occur during lift-off (137.9 dB) and transonic flight (135 dB) with a reference pressure of 0 dB ($2 * 10^{-5}$ Pa), but are substantially lower outside these periods [6].

Thermal Environment: In a typical suborbital flight profile, external conditions such as pressure and temperature undergo significant changes throughout all phases of the flight. A suborbital launch vehicle using compressed gases may have to overcome cold external temperatures and internal cabin cooling caused by pressurized gas release into the cabin [7]. During the SL-5 mission, a suborbital rocket spent approximately 1.8 minutes above the Karman line and experienced temperatures ranging from 26 ^{o}C to 49 ^{o}C, with an estimated maximum of 66 ^{o}C [8].

Radiation: Up to an altitude of 90 km, the major constituents of the Earth's atmosphere remain relatively stable. However, beyond this point, the composition and amounts of gases changes. These gases are affected by shortwave solar radiation, leading to various photochemical effects where molecules undergo structural changes upon absorbing radiant energy [9]. In the suborbital space, the radiation environment

comprises trapped radiation in Earth's magnetic field, background galactic cosmic radiation (GCR) and occasional intense solar energetic particle events. The most severe radiation flux that suborbital flights could be exposed to is beyond ~100 Mega electron Volts (MeV) [10].

EFFECTS OF ORBITAL SPACE ENVIRONMENT ON STRUCTURAL COMPONENTS

Spacecraft circle Earth in different orbits under the influence of gravity. The three main orbits are classified as geostationary Earth orbit (GEO), that is 36,000 km above the equator; medium Earth orbit (MEO), between GEO and LEO; and low Earth orbit (LEO), 200 – 1,000 km above Earth. Satellites used mostly for Earth observation and manned spacecraft such as the International Space Station operate on LEO [11].

Thermal Environment: Temperature variations in space results in thermal cycling of structures. When a vehicle spins in space, it receives heat from the sun while dissipating heat to deep space since the sun's heat radiation comes from a fixed direction [12]. To prevent system fatigue, changes in temperature must be minimized as orbital temperature varies over orbits and mission lifetime. Temperature fluctuations may lead to the fatigue of delicate wires and solder joints, potentially causing system failures. Objects exposed to LEO space may encounter temperatures as low as -120 ^{o}C and as high as 150 ^{o}C. Enclosed payloads in LEO are expected to encounter a temperature range of -10 ^{o}C to 55 ^{o}C [8, 9].

Radiation: Energetic trapped particles and cosmic rays could generate background noise in sensors and detectors while masquerading as real signals which may affect subsystems [13]. Space radiation sources are trapped radiation belt (Van Allen belt) particles, cosmic rays and solar flare particles. The radiation environment consists of high-energy particles that can travel through spacecraft material and deposit kinetic energy, leading to atomic displacement or the generation of charged atoms. In Van Allen Belts, naturally occurring radiation ranges from 10 keV to over 30 MeV for a solar event. On LEO, radiation doses can be approximately 1.0 Gy/yr (0.1 krad/yr) when shielded by a 2.5 mm thick aluminum case [8, 9, 11].

Vacuum: Space is considered to be a vacuum beyond Earth's atmosphere. This vacuum environment causes out-gassing, cold welding and heat transfer from radiation. In some cases, the gasses that escape during outgassing can coat delicate sensors, or cause electronic components to arc, resulting in damage. The in-flight pressure expected for a flight hardware in LEO is 10^{-10} Torr [14, 15].

Oxygen: Temperature, density and composition in the thermosphere are very sensitive to solar cycle due to the absorption of extreme ultraviolet radiation from the sun. Atomic oxygen, a major constituent of the low-Earth orbit (LEO) thermosphere, poses a threat to spacecraft materials [8]. When exposed to AO, the surfaces of spacecraft in LEO can undergo surface breakdown, leading to weakened components, altered thermal characteristics, and degraded sensor performance [14, 16].

Space Debris: Rocket and satellite structures are susceptible to damages from debris and meteoroids caused by human activity in space. The hypervelocity impact of these objects on space structures could induce a shock environment that is close to those generated by pyroshock devices, with the velocity of micrometeoroids reaching 20 km/s and those of orbital debris reaching 15 km/s [17]. Electrical components of

a payload, are usually miniature and therefore have high resonant frequencies which make them exposed to damage by pyroshock [18].

DYNAMIC MODEL OF PZT WITH THERMAL AND RADIATION EFFECTS

Previous studies investigated the effect of temperature on the resonant frequency of PZT sensors. Lee et al [19] showed that the resonant frequency decreased steadily from 47.5 kHz at −100 ^{o}C to a minimum value at the room temperature of 22 ^{o}C and then started to increase to 44.0 kHz at 90 ^{o}C. The same tendency was observed in the anti-resonant frequency. Upadhye and Agashe [20] measured the resonant frequency of PZT 4 and PZT 5 sensors between 5 ^{o}C and 50 ^{o}C, it was observed that as the temperature increases the resonant frequency decreases. This was because the resonant frequency of the piezoelectric element is directly proportional to stiffness constant and as the temperature of the piezoelectric element increases, its stiffness decreases leading to a decrease in the resonant frequency. Baptista et al [21] also showed experimentally that the resonant peak frequency of PZT-5H sensor decreases as the temperature increases from 25 ^{o}C to 102 ^{o}C.

Previous work shows that temperature variations affect the modulus of elasticity of materials, especially in metals. Generally, an increase in temperature leads to a decrease in the modulus of elasticity of most materials [22]. Grisso et al [23] modified the equations for determining damage based on a longitudinal wave by Kabeya et al [24] by introducing the effects of temperature variation on a structure. The wave speed is a function of Young's modulus, which deteriorates as temperature increases. When temperature exceeds 200 ^{o}C, the wave speed needs to be recalculated to account for this deterioration. An equation for determining the temperature corrected modulus of elasticity was developed such that the wave speed does not need to be recalculated. Silverman [25] explored the factors to be considered in spacecraft thermal control system design. These factors are allowable operating temperatures, mission modes, energy absorption, internal and external heat generation. For most components of a spacecraft, the allowable operating temperature ranges between -184 ^{o}C to 121 ^{o}C. External radiation sources are the sun, albedo, and earth emission, impacting thermal design due to coatings and surfaces' response. Internal heat generation comes from the payload and support equipment, it is managed by insulating coatings and careful component placement. Gamma radiation affects the EMI of aluminum and PWAS by causing a forward frequency shift with increasing exposure levels [26]. The goal of the present contribution is to develop a model accounting for thermal and radiation effects.

The extensional vibration of the radial symmetric mode in a thin circular disc is described by the set of three equations in (1).

$$T_{\mathrm{rr}} = \mathrm{c}'(S_{rr} + \sigma S_{\theta\theta}) - \mathrm{e}'E_{\mathrm{z}}, \quad T_{\theta\theta} = \mathrm{c}'(\sigma S_{rr} + \sigma S_{\theta\theta}) - \mathrm{e}'E_{\mathrm{z}}, \quad D_{\mathrm{z}} = \epsilon_{33}^{PS}E_{\mathrm{z}} + \mathrm{e}'(S_{rr} + S_{\theta\theta}) \tag{1}$$

where $c' = \frac{1}{s_{11}^{E}(1-\sigma^2)}$, $\sigma = -\frac{s_{12}^{E}}{s_{11}^{E}}$, and $e' = \frac{d_{31}}{s_{11}^{E}(1-\sigma^2)}$.

Since the mode is axially symmetric and $u_\theta = 0$, $S_{rr} = \frac{\partial u_r}{\partial r}$ and $S_{\theta\theta} = \frac{u_r}{r}$; the

coupling coefficient is

$$k_p^2 = \frac{2\, d_{31}^2}{(1-\sigma)(s_{11}^E \epsilon_{33}^T)} \tag{2}$$

From the last equation in (1), we obtain

$$\epsilon_{33}^{PS} = \epsilon_{33}^T (1 - k_p^2), \tag{3}$$

where *p* represents planar expansion and PS indicates planar clamped. Equation (1) leads to

$$-\omega^2 \rho u_r = \frac{\partial T_{rr}}{\partial r} + \frac{T_{rr} - T_{\theta\theta}}{r} = c'\left(\frac{\partial^2 u_r}{\partial r^2} + \frac{\partial u_r}{r \partial r} - \frac{u_r}{r^2}\right) \tag{4}$$

The solution for u_r is sought in terms of Bessel functions. Sound velocity $v = \frac{1}{[\rho {s_{11}}^E (1-\sigma^2)]^{\frac{1}{2}}}$.

Applying stress free boundary condition at *r=a* and considering electrical displacement D_z the admittance can be found to be

$$Y = Y_0 + Y_p\,, \qquad Y_0 = j\omega C_0, \qquad C_0 = \epsilon_{33}^{PS} \pi a^2 / t \tag{5}$$

$$Y_p = j\omega C_0 \frac{k_p^2}{1-k_p^2} \frac{1-\sigma}{\frac{x J_0(x)}{J_1(x)} - (1-\sigma)}, \qquad Z = Y^{-1} \tag{6}$$

where $x = \frac{\omega a}{v}$. At resonance, the denominator of equation (6) equals zero.
Therefore, the resonant angular frequency of the nth order is given by

$$\omega_{Rn} = \frac{R_n}{a} \left(\frac{1}{\rho {s_{11}}^E (1-\sigma^2)}\right)^{1/2} \tag{7}$$

where Rn is the roots of the denominator of equation (6) i.e $\frac{x J_0(x)}{J_1(x)} = (1-\sigma)$.
The analytical solution (5, 6) can be presented in terms of the electrical circuit equivalent depicted in Figure 1a and described by expressions (5) and (8).

$$Y_p = \sum_n [j\omega L_n - j/(\omega C_n)]^{-1} \tag{8}$$

where $C_n = C_0 \cdot p_n \cdot \frac{k_p^2}{1-k_p^2}$, $L_n = 1/({\omega_{Rn}}^2 \cdot C_n)$, $p_n = \frac{2\cdot(1+\sigma)}{{R_n}^2 - (1-\sigma^2)}$

The results of modeling using Eqs. (5, 6, 8) for a 7mm PZT-5A ceramic sensor and the associated comparison with experimental data is presented in Figure 1b. The discrepancy for the impedance peak seen for the circuit model is attributed to a limitation on one-contour circuit with C_0, C_1, L_1 only. As more contours (modes) are considered, the electrical model fits the analytical model. Additional elements C_{1T}, $L_{1T...}$ are considered as contribution of temperature and radiation effects.

THERMAL CHAMBER EXPERIMENT

The electromechanical impedance of a free PZT sensor was measured at temperatures ranging from room temperature to 240 ^{o}C. Lead wires were soldered to a PZT sensor using a 99.3%Tin/0/7% Copper (lead-free) solder that is able to withstand temperatures up to 227 ^{o}C. The sensor is APC-851 PZT 5A with a diameter of 7 mm and a thickness of 0.25 mm. The sensor was placed in an ADP300C vacuum drying oven and the temperature was incrementally increased from room temperature at 22 ^{o}C to 240 ^{o}C with steps of 10 ^{o}C. The sensor was allowed to settle at each temperature for approximately one hour before impedance measurements were taken. The impedance of the sensor was measured at each temperature in a frequency range of 290 kHz to 380 kHz with 1024 points using the Cypher Instruments' C60 impedance-amplitude-phase analyzer. Figure 2a shows a plot of the real part of the impedance of the sensor.

The plot in Figure 2b shows that the natural frequency of the sensor shifted downwards from 339 kHz at room temperature to 330.5 kHz at 140 ^{o}C, after which it started to increase to 38.4 kHz at 230 ^{o}C. The in-plane anti-resonant and resonant frequencies of the PZT-5A sensor was determined from the phase angle of the experimental results. Figure 2**Error! Reference source not found.**b shows the anti-resonant frequencies of the sensor at varying temperatures which better illustrates trend visible in Figure 2a. The anti-resonant frequency decreased as the temperature increased from room temperature to 140 ^{o}C and then increased to 240 ^{o}C. It is apparent from the figure that frequency dependence on temperature exhibit quadratic dependency and the equation of fit resulted in $f_{AT} = 0.008*T^2–0.2199*T+331.6793$. This trend can be used in combination with the electric circuit model in Figure 1a to predict behavior of piezoelectric sensors under environmental conditions of spaceflight. The circuit includes additional circuit elements representing quadratic temperature dependency and linear frequency dependency on radiation effects [26]. Assuming temperature independence of the radiation effects, this results in the upward shift of the quadratic curve in Figure 2b as the radiation dose increases.

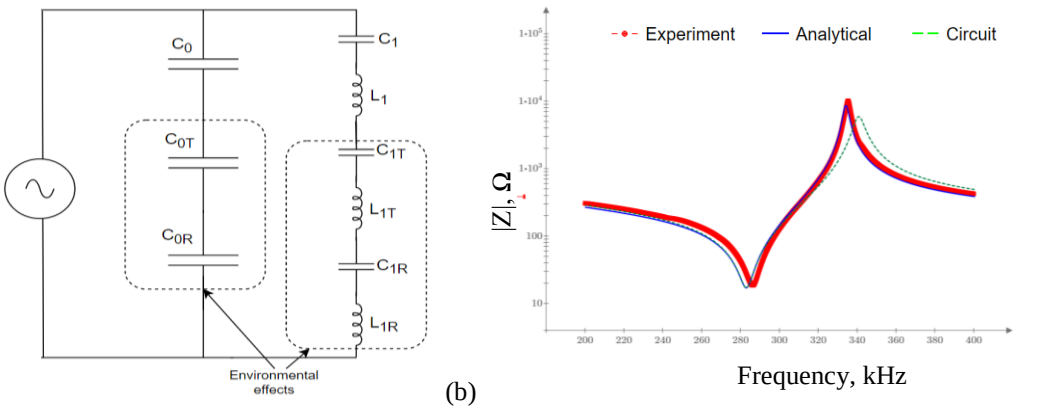

Figure 1. (a) Equivalent electrical circuit model of PZT with environmental effects, (b) comparison of experimental data to analytical and electrical circuit models.

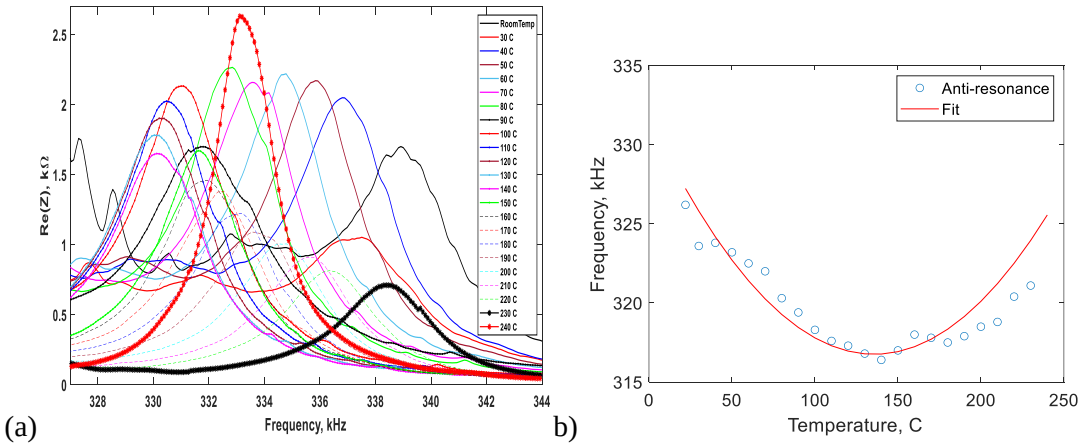

Figure 2. a) Electromechanical impedance of the PZT sensor at increasing temperatures. b) Anti-resonant frequencies of APC 851 sensor at varying temperatures

CONCLUSIONS

Structures in a sub-orbit and in space are affected by different environmental factors such as vibrations, temperature variations, radiation, atomic oxygen, vacuum, acoustic load, micrometeoroids and debris, etc. The effect of temperature on materials in LEO was considered in this paper. An experiment was carried out to determine the effect of temperature on APC 851 PZT 5A sensor. Results showed that the anti-resonant frequency of the sensor shifts downwards from room temperature to 140 ^{o}C and then upward beyond 140 ^{o}C. A quadratic dependency of the anti-resonance frequency on temperature was observed and the associated equation was proposed. An electric circuit model of the sensor is suggested. This model may be used to account for changes in natural frequency of the piezoelectric sensor due to quadratic temperature effects and linear radiation effects.

ACKNOWLEDGEMENT

The financial support of NASA ISS EPSCoR program is gratefully acknowledged.

REFERENCES

1. Pisacane, V. L. 2008. “The Space Environment and its Effects on Space Systems,” American Institute of Aeronautics and Astronautics. ISBN 978-1-56347-926-7
2. Bedingfield, K. L., Leach, R. D., and Alexander, M. B. 1996. “Spacecraft System Failures and Anomalies Attributed to the Natural Space Environment,” NASA Ref. Publ. 1390, Marshall Space Flight Center, AL.
3. Mann, A. (2020). “What’s the difference between orbital and suborbital spaceflight?” https://www.space.com/suborbital-orbital-flight.html. Accessed on April 24, 2023.
4. Nwokocha, F., Zagrai, A., Hunter, D., Amon, D., and Demidovich N. 2022. “Electro-mechanical Impedance Experiment and Real-time Data Acquisition for Suborbital Spaceflight,” SHM 2021.
5. Mandell, G. K., Caporaso, G. J., and Bengan, W. P. 1973. “Topics in advanced model rocketry” Cambridge, Mass., MIT Press. xviii, 631, ISBN : 0262020963

6. Shakir, A. B., Ez-Deen, S. Y. 2009. “Effect of acoustic vibration on the satellite structure at launch stage”. *International Conference on Modeling and Simulation*. 32-37.
7. FAA. 2010. “Environmental Control and Life Support Systems for Flight Crew and Space Flight Participants in Suborbital Space Flight,” Environmental Control and Life Support Systems – Guidance V. 1.0
8. Zagrai, A. et al., 2012. “Active structural health monitoring during sub-orbital space flight,” *The Journal of the Acoustical Society of America*, vol. 132, 1964.
9. James, B. F. 1994. “The natural space environment: effects on spacecraft”. National Aeronautics and Space Administration (NASA) Reference Publication 1350
10. Anderson, M., Zagrai, A.N., Daniel, J.D., Westpfahl, D.J., Henneke, D., 2017. “Investigating Effect of Space Radiation Environment on Piezoelectric Sensors: Cobalt-60 Irradiation Experiment,” *Journal of Nondestructive Evaluation, Diagnostics and Prognostics of Engineering Systems 1*, 011007-011007–11.
11. Yang, J. C. and de Groh, K. K. 2010. “Materials Issues in the Space Environment,” *MRS Bulletin*, vol. 35, no. 1, pp. 12–19.
12. Gadalla, M. A. 2005. “Prediction of temperature variation in a rotating spacecraft in space environment” Applied Thermal Engineering 25:2379-2397.
13. Lauriente, M., Vampola, A. L., Koga, R. and Hosken, R. 2012. “Analysis of spacecraft anomalies due to the radiation environment”. Journal of Spacecrafts and Rockets. 36(6):902-906
14. FAA. “The space environment”, Advance Aerospace Medicine On-line
15. Jeannette Plante and Brandon Lee (2004). “Environmental Conditions for Space Flight Hardware – A Survey” *For the NASA Electronic Parts and Packaging (NEPP) Program, 2004, Dynamic Range Corporation.*
16. Vampola, A. L. 2012. “Analysis of environmentally induced spacecraft anomalies” Journal of Spacecrafts and Rockets. 31(2):154-159
17. Pavarin, D. et al. 2005. “Analysis of Goce’s Disturbances Induced by Hypervelocity Impact”. *Proceedings of the Fourth European Conference on Space Debris, Darmstadt, Germany*, (ESA SP-587)
18. Patrick L. Walter “Pyroshock Explained” https://www.pcb.com/contentstore/MktgContent/Linkeddocuments/Technotes/TN-23_Pyroshock_Explained.pdf PCB Piezotronics. (visited on 05/04/2023)
19. Lee, S., Kim, M., Kim, J., and Yoo, S. 2012. “Equivalent circuit with temperature parameters for piezoelectric sensor under space environment”. 2012 *IEEE International Ultrasonics Symposium Proceedings*.
20. Upadhye, V., and Agashe, S. 2016. Effect of temperature and pressure variations on the resonant frequency of piezoelectric material”. *Journal of Measurement and Control*, 49(9) 286-292.
21. Baptista, F. G., Budoya, D. E., de Almeida, V. A. D., Ulson, J. A. C. 2014. “An experimental study on the effect of temperature on piezoelectric sensors for impedance-based structural health monitoring”. *Sensors Journal*, 14:1208-1227.
22. Hooker, M. W. 1998. “Properties of PZT-based piezoelectric ceramics between -150 and 250^{o}C NASA/CR-1998-208708.
23. Grisso, B. L., Leo, D. J., and Inman, D. J. 2004. “Temperature influences on the wave propagation technique for use in supplementing impedance-based structural health monitoring,” Proc. SPIE 5394, 222-232.
24. Kabeya, K., Jiang, Z., and Cudney, H. H. 1998. “Structural Health Monitoring by Impedance and Wave Propagation Measurement,” Proceedings of International Motion and Vibration Control, 207-212, Switzerland.
25. Silverman, E. M. 1995. “Space environmental effects on spacecraft: LEO materials selection guide,” NASA contractor report 4661, contract NAS1-19291
26. Anderson, M. L., Daniel, J. D., Zagrai, A. N., and Westpfahl, D. J. 2017. “Electro-Mechanical Impedance Measurements in an Imitated Low Earth Orbit Radiation Environment,” ASME International Mechanical Engineering Congress and Exposition.